MAKING THE MOST OF ROD DESIGN - A COMPARISON OF MEASURED AND MODELED ROD STRING STRESSES

R.E. Ott, Mobil Exploration & Producing U.S. Inc.
G.L. Mendenhall, Texland Petroleum Inc.

ABSTRACT

Several software programs are available to calculate a pump downhole load-position card from dynamometer data. Most of these programs use the wave equation, with various solutions (Fourier Series, Method of Characteristics, Finite Differences, etc.) to help set damping conditions. A downhole tool with strain gauges is available to measure the actual forces at the pump as well as mid-string. Use of this tool has led to providing actual downhole values much less than those predicted by the software programs. This paper will present the actual data collected by this downhole lead cell. This data will then be compared to load values calculated by these commercially available software programs.

BACKGROUND

With the release of more sophisticated software programs, the question arises as to the relative strengths and weakneses of each. The wave equation is relatively straight forward, but solutions may be developed in several ways according to the asumptions made. Because different software programs treat these assumptions differently, which program to select for a particular downhole assembly may become important. The only way to verify the accuracy of the various software programs is to gather empirical data of the actual downhole load or force values.

This paper addresses validation of various computer programs as well as accurate rod stress predictions for buckling analysis.

INTRODUCTION

There has always been a demand for optimizing pumping systems to:

- Maximize production;
- Increase longevity of the system (not just make it work); and
- Minimize operating costs.

Consideration of these items should lead to a smooth, economical operation of a beam-pumping unit well. In today's operating environment, all of these factors have to be examined.

This paper was prepared for presentation at the 1994 Permian Basin Oil & Gas Recovery Conference held in Midland, Texas March 16-18, 1994.

A downhole tool has been available for several years which will measure the actual forces that occur where the tool is installed. To date, use of this tool to gather relevant information to examine software predictive programs had been ignored.

Mobil Exploration and Producing U.S., Inc. (MEPUS) decided to obtain downhole force data at both the bottom of the rod string as well as in the middle of the rod string. Both of these areas can be critical in the design of the rod string. Excessive compression forces can lead to premature failures in the well, which will greatly increase operating costs. With the use of the downhole tool, the data gathered was compared to several existing software programs as well as the API 11L calculations. These interpretations have resulted in a more efficient and optimized rod string design.

The Downhole Load Cell (DHLC) tool has direct application for assessing and developing models for shallow, viscous oil wells and deviated, high friction wells. Also, the tool can be used in the development of two-stage pump Bottom-Up models.

DOWNHOLE LOAD CELL (DHLC) EQUIPMENT

The Downhole Load Cell (DHLC, Figure 1) is used to gather the empirical data for these tests. The DHLC consists of a pressure transducer, strain gauge load cells, and a microprocessor with a timetable and a calibration phase. Glenn Albert of Albert Engineering designed and developed the tools that were used in this work. These tools are an advancement of the pioneering effort conducted while he was at the University of Oklahoma.

The data is collected by a self-contained battery operated processor that is run on the rod string. Sampling is conducted at predetermined times while the tool is in the wellbore. Quantitative data is collected (usually four periods) at 50-60 Hz, and at other times the data is collected at a 10 Hz sampling rate.

The key to capturing valid data is to conduct a standing valve check while testing. The standing valve check will allow measurement of the weight of the pump below the tool when positioned at the bottom of the rod string. With this value known, the rest of the data gathered can be assessed and then compared to the solutions offered by the various software programs.

Usually standing valve tests were conducted during each test period to ensure there was no drift in the tool. If drift occured, it was corrected. During some of the tests, the beam unit was started up to observe the forces occurring downhole. A travelling valve check was conducted to confirm the load value as well. Results will be discussed later in the paper.

WELL TESTS AND CHARACTERISTICS

Data from four wells will be presented in this paper. These wells are located in the Four Corners area and the Permian Basin. Pertinent data on the four wells selected are presented, cases 1 through 4, in Table 1.

Wells chosen for the DHLC test program represent the most common lift designs for Mobil in West Texas, New Mexico, and Utah. The test wells range in depth from 5,300 to 6,400 feet. Production rates vary from 60 to over 560 BFPD. Plunger diameters also vary from 1.25 to 2.00 inches. The wells were tested so measured and modeled loads could be compared for their lift installations.

DISCUSSION OF RODSTRING MODELS

Two problems exist in the modeling of rod pumping systems. The first problem is the simulation of rod pumping systems for the purpose of design. This is known as the "Bottom-Up" model and is named as such because of assumed pump action. The rod dynamics and surface loads are calculated from this pump action.

The second problem is the diagnosing of an existing rod system where surface loads are physically measured. This is known as the "Top-Down" model. From known surface loads, rod dynamics and pump loads are calculated. Although each problem is solved differently, use of the DHLC tool is relevant to both in acquiring accurate solutions.

Generally, two mathematical models are used to represent rod pumping systems. These models are the one dimensional, damped wave equation and Newton's linear equation of motion for a lumped system. The wave equation is a second order, hyperbolic partial differential equation which describes the motion of standing waves. The equation of motion for a lumped system is a second order differential equation which describes the motion of a discrete number of elements under forced, harmonic motion. Both models are valid for harmonic, steady state, forced linear systems and rely on viscous damping in the simulation of rod string and pump motion. The wave equation approach is the most common in industry today.

In a simplified form, the wave equation is given by:

$$v^2 \frac{\partial^2 u}{\partial x^2} = \frac{\partial^2 u}{\partial t^2} + c \frac{\partial u}{\partial t} \quad \ldots\ldots \text{Eq. } 1^5$$

where v is the velocity of force propagation in the rod string material. In simplified form, Newton's equation of motion is given by:

$$m \frac{\partial^2 x}{\partial t^2} + c' \frac{\partial x}{\partial t} + kx = 0 \quad \ldots\ldots \text{Eq. } 2^{[5]}$$

where k is an elastic spring constant for the rod string material. The other terms in these equations are defined at the end of the paper.

In the comparison of seven software programs (Models A-G below), three solution techniques were used. The techniques consist of the use of finite differences, Fourier series, and the method of characteristics to solve the wave equation. For the "Bottom-Up" case, three solution techniques are also used. The models involve two solutions with a finite difference technique to the wave equation and one with a lumped, discrete technique to the equation of motion. Lastly, the rodstring solution in API's RP11L is included for reference.

The software programs are labelled as follows:

Top-Down

Model A - Finite Difference
Model B - Characteristics
Model C - Fourier Series

Bottom-Up

Model D - Finite Difference
Model E - Lumped Analysis
Model F - Finite Difference
Model G - API RP11L

DISCUSSION OF SOLUTION TECHNIQUES

It is not the intent of this paper to present the details of the mathematical models and solution techniques. However, it is important that these methods be understood by rod system designers and trouble-shooters.

Finite difference solutions are used in Models A, D, and F. The use of finite differences is a valid method of obtaining a numerical solution to the one dimensional, linear hyperbolic wave equation. This method assumes periodic (steady-state) solutions, so only two boundary conditions are required. The models are based on the use of Taylor Series approximations to generate finite difference analogs for the displacement derivatives in the wave equation. This method affords flexibility in tapered and multi-material rodstrings. Also, this method offers direct determination of truncation error. The solution can be matched to rod taper lengths, so no interpolation at taper changes is necessary. Increasing data sampling in the Top-Down model yields higher resolution of pump loads. However, numerical solutions at matching higher resolution requires greater computation time.

Two limitations exist in the finite difference method. First, the solution is dependent on an energy dissipating damping coefficient (validated only by downhole measurement). Second, finite differences typically can not resolve a "ringing" effect when sudden load reversals occur. Data smoothing or fast integration can be necessary for the model to make physical sense. Thus, some resolution can be lost. In the Bottom-Up models, the solution is dependent on accurate pump condition predictions. When predicted poorly, surface loads can deviate greatly from measured loads.

A method of characteristics solution is used in Model B. The method of characteristics is another numerical approach to the one dimensional, linear hyperbolic wave equation. This method introduces auxiliary functions which greatly simplify the wave equation solution through translation to a characteristic coordinate system (eigenvalue matrix). The method is flexible in allowing time and depth dependent damping coefficients. Also, the method yields straight forward solution error estimates. Computational time is greatly decreased in this method because of the simplified integration scheme used for solution.

As with other methods, the method of characteristics model relies on an equivalent damping factor, validated only through actual stress measurement. Also, since surface data is measured at uniform time intervals, a specific rodstring length interval is dictated by the solution characteristic slope. Therefore, interpolation is necessary to determine loads and positions at rod diameter and material changes if the interval does not coincide with solution nodes. The interpolation and simplification yields some undetermined error in the solution.

A Fourier series solution is used in Model C. The model is based on the use of Fourier series trigonometric expansions to solve the wave equation. The model takes measured surface loads, polished rod positions, and times, and generates a Fourier series approximation. Using Fourier series representations of boundary conditions and various intermediates, including displacement and force coefficients, the dynamic load is determined as a function of both time and depth. Although this method represents an exact analytical solution when an infinite number of terms is included, in practice, only 10 to 16 terms are used.

Although the Fourier series method is widely used in the Top-Down problem, some errors are inherent to this technique. Truncation error estimates are difficult to define. Also, since a Fourier series approximation of polished rod load results in data smoothing at the onset, resolution is immediately sacrificed. As the solution is transmitted downhole, resolution is lost as well. The loss of resolution can be greater than with other methods. High resolution is important in determining cyclical load variations from higher order harmonics.

Exclusively a Bottom-Up solution, Model E, uses a solution of the equation of motion. The discretized, lumped analysis approach dissects the rodstring into separate masses, dampeners, and springs. Newton's second law is applied to the discretized rod string, yielding second order differential equations of motion. Redefining variables yields first order differential equations. When considered with downhole pump boundary conditions, these equations are readily solved with improved computational speed.

Several concerns are relevant to discretized, lumped analysis. For example, the optimum number of discretized elements cannot be determined without experimental verification. Also, weighted discrete analysis must be defined where rod diameter and material changes occur. This method is directly dependent on the natural frequency of the combined rod string (as is API RP11L's solution). Lastly, this model cannot yield accurate results when pumping frequencies are larger than the fundamental frequency of vibration of the rodstring. (Fortunately, most systems are operated at less than half of the natural frequency.) Model G is based on test data correlations as outlined in the RP11L. This method can be considered interpolative from the original electric analog model results. Readers are referred to API's recommended practice for further information on this method. Limitations are readily identifiable with this approach.

Unless a mathematical model is greatly simplified and solved analytically, models involving differential equations must be solved through numerical analysis. Models A through F are solved numerically. In these numerical solutions, three main sources of error occur. These sources are input, truncation, and roundoff errors. Input errors occur when measured values or assumed values are inexact. Truncation errors occur in an algorithm when polynomial or trigonometric expansions are used. Usually, error bounds can be determined for the algorithm being employed. Roundoff errors occur because computer hardware operates on a fixed number of digits. Excess digits are lost in multiplication and division operations. Input and truncation errors can be significant, destroying solution accuracy. The fact that no model yields an exact analytical solution must be understood from the outset. For the first time, equipment exists to accurately determine downhole forces. These values can then be used to compare to the predictive models.

DHLC RESULTS

The DHLC measured pump loads demonstrate the complexity of rod string simulation. Case #1-downhole (Figure 2) is the load versus time plot. Pump loads are initially as high as 3,850 lbs. during the onset of the upstroke and drop to 3,000 lbs. at the end of the upstroke. During the transition from upstroke to downstroke, two load reversals are seen (from 11.0 to 11.5 seconds). As the plunger travels through the downstroke cycle, the maximum compressive dynamic load is 300 lbs. This load occurs midway through the downstroke where the plunger velocity is greatest. The peak pump discharge pressure occured at the end of the downstroke. This was not expected.

This phenomenon is probably due to wave dynamics in the produced fluid. Thus, fluid inertia and compression effects are tied to plunger loading.

For Case #1-surface (Figure 3) the surface load versus time is plotted. Along with the surface load, the pumping unit's influence on loading from surface acceleration is demonstrated. Case #1-midstring (Figure 4) presents the midstring load versus time plot. The loads are measured at the fiberglass and steel rod interface. The midstring load plot mirrors the surface load plot.

Case #2-downhole (Figure 5) is the pump load and pressure versus time plot. In this all steel string, the pump card has a different nature than in Case #1. The pump loading is more uniform with a peak upstroke load of about 5,400 lbs. and a minimum upstroke load of 5,300 lbs. During the upstroke, the plunger stalls with a slight reversal in direction and then completes the upstroke. Also, the plunger experiences three load reversals on the upstroke to downstroke transition. These reversals appear to be caused by higher harmonics and standing wave travel through the rodstring. These load reversals are also seen on the downstroke to upstroke transition. On the downstroke, the maximum compressive load is about 200 lbs. Once again, the pump discharge pressures do not behave as expected. Similar to Case #1-downhole (Figure 2), the discharge pressures have a distinct amplitude period, with the maximum pressure occurring during the first half of the downstroke. The pressure fluctuations are integral to defining pump loads.

Case #3-downhole (Figure 6) presents a different pump load and pressure versus time plot. The loading is very much like Case #2-downhole. In Case #3, the upstroke maximum load occurs immediately at the beginning of the upstroke (4,050 lbs.). The load drops to about 3,550 lbs. just prior to a 1,000 lb. load reversal. Then, the load increases to over 3,700 lbs. at the end of the upstroke. During the upstroke to downstroke transition, several load reversals appear probably due to rodstring harmonics. On the downstroke, the maximum compressive dynamic load is about 150 lbs. Plunger velocity changes during the downstroke are apparent in the load fluctuations on both the up and down strokes. As for Case #2, the maximum pump discharge pressure in Case #3 occurs during the first half of the downstroke. The discharge pressure curve exhibits a steady state amplitude period.

Yet another different example, Case #4-downhole (Figure 7) is the pump load and pressure versus time plot. In this case, a different load cell configuration was used. The transitional dynamics are not observed. This could be the result of inadequate resolution to identify harmonic load transitions. However, the basic character of the load curve and pressure curve exist. As seen in the figure, the peak upstroke load is about 9,000 lbs. This peak load occurs after the initial upstroke displacement. A load transition occurs during the upstroke with a second peak load of about 8,400 lbs. During the downstroke, the minimum compressive dynamic load is about 350 lbs.

As in Cases #2 and #3, the maximum pump discharge pressure occurs during the downstroke (about 2,700 psi). However, the maximum pressure appears during the second half of the downstroke displacement. This indicates that the fluid dynamics are related to the pump's load plot.

MODEL PREDICTIONS COMPARED TO MEASURED RESULTS AND CALCULATIONS

During the study of the different modeling schemes, several important considerations must be reviewed. These considerations are the differences in Top-Down and Bottom-Up system loads. Gearbox and unit structure loading are both dependent on predicted polished rod loads in the Bottom-Up problem. In the Top-Down problem, gearbox and structure loading are dependent on actual measured surface loads. In Table 2, Case #1, models A through C predicted gearbox and structure loading to within 5 percent. Models D through F predicted gearbox and structure loading to an 8 percent and 7 percent variation, respectively. This result is as expected since models A through C rely on actual measured surface polished rod loads, while models D through F rely on predicted loads.

In Case #2 (Table 3) the difference is 2 percent and 0 percent for the Top-Down models, and 6 percent and 3 percent for the Bottom-Up models. Cases #3 and #4 yield slightly different results due to algorithm and dynamometer measurement errors. Case #3 (Table 4) gearbox and structure loading model differences are 5 percent and 4 percent, respectively for models A through C, and 6 percent and 3 percent for models D through F. This result indicates the Bottom-Up models are predicting structure loading with less difference than the Top-Down models. In Case #4, (Table 5) gearbox loading varies by 4 percent in models A through C, while varying only 1 percent in models D through F. This result shows the Top-Down models are relying on dynamometer measurements.

Another interesting result of the model comparisons is the Modified Goodman Diagram (MGD) load range difference. For Case #1 (Table 2) with two tapers (fiberglass and steel), the top rod section MGD loading varies by +3.3 percent for models A through C, and +5.7 percent for models D through F. For the bottom rod section, the Top-Down MGD load difference is +8.7 percent, while the Bottom-Up difference is +8.3 percent. This difference indicates that models D through F are predicting downhole loading to a tighter tolerance than the models relying on actual measured surface loads. This effect is expected since Bottom-Up solutions originate from the pump loading boundary conditions. In the other three cases, review of the results shows that for both sets of models, the greatest differences usually occur midstring.

The largest difference in model output appears in the gross plunger stroke. For Case #1 (Table 2), Top-Down and Bottom-Up differences are 13.4 percent and 17.5 percent, respectively. These differences give greatly differing production predictions. In Case #2 (Table 3), these differences are 2.2 percent and 20.0 percent, respectively. For Case #3 (Table 4), the differences are 7.3 percent and 6.8 percent, respectively. And for Case #4 (Table 5), the differences are 0 percent and 1.3 percent, respectively. Thus, all steel rodstring Top-Down models demonstrate consistent results. The fiberglass rodstring (Case #1) yields the greatest difference in the Top-Down prediction.

DETERMINATION OF DYNAMIC FORCE

Another important consideration in using the DHLC is the accuracy of rodstring models in predicting rod buckling. The results of each model are presented in different formats. The design engineer must be aware of the form in which a computer program's output is given so that a buckling analysis is useful. For example, in the models used, three different presentations are seen. Output data was given as the bottom minimum stress (psi), dynamic stress (psi), and bottom minimum force (lbs). The bottom minimum stress and force outputs include hydrostatic effects while the bottom minimum force output removes the hydrostatic effects. In buckling analysis, bi-axial stress analysis yields hydrostatic effect cancellation. In other words, hydrostatic effects can negate themselves. The pertinent stress then is only dynamic stress without hydrostatic effects. Tables 2-5 present comparisons between the DHLC measured and the modeled pump loads. Predicted results are annotated to demonstrate the variety of output presentations.

On review of the dynamic force predictions, the load differences appear excessive. However, by adjusting the zero force baseline to coincide graphically with the beginning of the downstroke (see Figure 8), a relative compressive load can be determined. This adjustment is necessary for the Top-Down models because of errors in dynamometer load cell measurements and rodstring buoyant weight calculations. For Case #1 (Table 2), peak and minimum polished rod measurements vary by 580 lbs. and 196 lbs., respectively, giving considerable difference in the dynamic loads of models A through C. Even greater error in measurement is seen in Case #4, where peak and minimum polished rod measurements vary by 1,331 lbs. and 1,450 lbs., respectively. This measurement error results in a tensile force on the downstroke (actually compressive by DHLC measurement). Therefore, an adjusted baseline is absolutely necessary to eliminate errors introduced from measurement.

In the Bottom-Up models, only model D can be manipulated. The difference in model D appears from errors in the pump boundary condition and errors in truncation only. Models E and F yield a zero compressive load by algorithm design and are useless in any buckling analysis.

Where the measurement error is minimum, adjustment of the baseline yields acceptable results for the Top-Down models. For Case #2 (Table 3), the compressive load difference from DHLC measurements is only about 13 lbs. For Case #3 (Table 4), the difference is 57 lbs. These results are sufficiently accurate for a relevent buckling analysis. However, because of the measured load errors in Cases #1 and #4, the Top-Down algorithms have skewed the bottomhole dynamic load results. In Case #1, the dynamic compressive load difference from DHLC measurement is 258 lbs. For Case #4, the difference is 195 lbs. These results are not within acceptable accuracy for the purpose of design changes, but may be qualitatively useful for problem diagnosis. Downhole dynamic force determination is dependent on surface load measurement accuracy in the Top-Down problem and on pump boundary conditions in the Bottom-Up problem.

CONCLUSION

The DHLC tool has provided a means of determining computer modeling program accuracy. Most models yield acceptable results when input errors are minimized and damping factors are properly determined.

When input errors occur in the Top-Down models, excessive deviation between actual and predicted rod and pump loads is observed. Simplistic pump loading assumptions in the Bottom-Up models create unreliable design predictions.

In summary, the comparison between measured and modeled rod stresses and system loads demonstrates predictive and diagnostic models are acceptably accurate when calibrated to known loads. However, if a critical design is under consideration, close inspection of the model selected has to be made. When truncation error is determined for any commercial or in-house computer simulation program, input errors can be identified and corrected for improved model accuracy.

NOMENCLATURE

c = viscous damping factor, 1/seconds
c' = damping constant, lb_f/ft/sec
k = spring constant, lb_f/ft
m = lumped mass in rod string, lb_m
t = time, seconds
x = axial distance along rod string, ft
u = rod displacement, ft
v = velocity of force propagation, ft/sec

ACKNOWLEDGEMENT

The authors wish to thank the management of Mobil Exploration & Producing U.S., Inc. and Texland Petroleum, Inc. for permission to publish this work.

REFERENCES

1. Agnew, J. and Knapp, R.C., *Linear Algebra With Applications*, Brooks/Cole Publishing Company, Monterey, California, 1983, pp. 127-139.
2. *Recommended Practice for Design Calculations for Sucker Rod Pumping Systems*, API RP11L, 4/ed, American Petroleum Institute, Washington, D.C., June 1988, pp. 4-7.
3. Beyer, W.H., *CRC Standard Mathematical Tables 25/ed*, CRC Press, Boca Raton, Florida, 1978, pp. 35-38, pp. 460-466, and pp. 488-491.

4. Diprima, B., *Elementary Differential Equations and Boundary Value Problems*, John Wiley & Sons, New York, New York, 1977, pp. 344-345 and pp. 491-499.
5. Everitt, T.A. and Jennings, J.W., "An Improved Finite-Difference Calculation of Downhole Dynamometer Cards for Sucker-Rod Pumps", *SPE Production Engineering*, February 1992, pp. 121- 127.
6. Scheid, F., *Numerical Analysis 2/ed*, Schaum's Outline Series, McGraw-Hill Book Company, New York, New York, 1988, pp. 94-202.
7. Spiegel, M.R., *Fourier Analysis*, Schaum's Outline Series, McGraw-Hill Book Company, New York, New York, 1974, pp. 20-44.
8. Steidel, R.F. Jr., *Mechanical Vibrations 2/ed*, John Wiley & Sons, New York, New York, 1979, pp. 313-333 and pp. 365-377.

Table 1
Relevant Pumping Unit Data

DATA	CASE 1	CASE 2	CASE 3	CASE 4
Pumping Unit Data				
API Unit Designation	M456-365-144	C320-246-86	C320-250-84	C912-365-168
Manufacturer	Lufkin (Mark II)	American	Lufkin	Lufkin
Pumping Speed, SPM	11.45	10.21	11.0	8.86
Stroke Length, in	111.8	60.0	84.2	169.8
Rotation	CCW	CCW	CW	CCW
Production: oil (BOPD)	35	34	12	16
water (BWPD)	424	138	51	545
gas (MCFPD)	12	11	5	1
Run Time, hrs	24	24	14	24
Rod Data				
Dia. (in)	1.250 1.000	0.875 0.750	1.000 0.875 0.750	1.000 0.875 0.750
Length (ft)	2850 2850	2025 3350	1525 1525 3300	1400 1575 2625
Material	Fiberglass D Grade Steel	D Grade Steel D Grade Steel	D Grade Steel D Grade Steel D Grade Steel	High Strength Steel High Strength Steel High Strength Steel
Elasticity (psi)	7.2 x E6 30.5 x E6	30.5 x E6 30.5 x E6	30.5 x E6 30.5 x E6 30.5 x E6	30.5 x E6 30.5 x E6 30.5 x E6
Downhole Data				
Pump Depth, ft	5716	5387	6358	5608
Plunger Size, in	1.75	1.75	1.25	2.00
Pump Intake Pressure, psi	1019	351	408	109
Fluid Specific Gravity (-)	0.99	0.97	1.03	(-) 1.05

Table 2
Program Output Comparisons
Case 1

Item	DHLC	A	B	C	D	E	F	G
				MODELS				
Gearbox %	-	N/A	62	59	61	61	66	-
Unit %	-	46	46	44	48	46	49	-
PRHP (hp)	-	N/A	20.6	21.8	22.0	23.1	23.4	-
PPRL (lbs)	16772	16663	16772	16192	17700	16706	17739	-
MPRL (lbs)	3204	3056	3204	3008	4451	2941	3668	-
SPM	11.5	11.3	11.5	11.3	11.3	11.5	10.5	-
1.25" FG %	-	67	63	70	59	68	72	-
1" SR %	62	62	74	81	61	70	78	-
Pump Stroke								
Gross (in)	-	112	127	125	134	127	114	-
Net (in)	-	N/A	127	123	N/A	N/A	114	-
PPIP (psi)	1050	1817*	640	576*	1019	1050	576	-

* Calculated by Program

Item	DHLC	A	B	C	D	E	F
Bottom Min Stress (psi)	-2833	-7284*	-3885*	-4440	-3051	-2634*	-2636
Dynamic Min Stress (psi)	-382	-4833	-1434	-1662	-582*	-183	-185
Bottom Min Force (lbs)	-2225	-5721	-3051	-3487*	-2396	-2096	-2070*
Dynamic Force (lbs)	-300*	-3796	-1126	-1305	-457	-144	-145
Dynamic Force (lbs)	-300	-500	-500	-675	-150	0^	0^
Adjusted Baseline Gross Plunger Stroke (in)	N/A	112	127	125	125	127	114

* Program Output Value
^ Value Forced by Program Boundary Conditions

Table 3
Program Output Comparisons
Case 2

Item	DHLC	A	B	C	D	E	F	G
				MODELS				
Gearbox %	-	-	55	56	50	47	50	49
Unit %	-	-	71	71	60	68	67	65
PRHP (hp)	-	-	7.9	7.5	6.3	7.4	7.9	7.0
PPRL (lbs)	17383	-	17383	17556	16307	16713	16395	15901
MPRL (lbs)	6006	-	6006	6352	6080	6153	5301	6572
SPM	10.2	-	10.2	10.2	10.2	10.0	10.9	10.2
7/8" SR %	-	-	89	90	81	84	86	76
3/4" SR %	91	-	91	88	88	83	89	76
Pump Stroke								
Gross (in)	-	-	47	46	40	48	43	48
Net (in)	-	-	47	44	N/A	N/A	35	N/A
PPIP (psi)	351	-	350	451*	351	200	217	200

* Calculated by Program

Item	DHLC	A	B	C	D	E	F
Bottom Min Stress (psi)	-2716	N/A	-3532*	-2408	-2807	-2433*	-3950
Dynamic Min Stress (psi)	-453	N/A	-1269	-145	-544*	-170	-1686
Bottom Min Force (lbs)	-1200	N/A	-1560	-1064*	-1238	-1075	-1745*
Dynamic Force (lbs)	-200*	N/A	-561	-64	-240	-75	-745
Dynamic Force (lbs)	-200	N/A	-250	-175	-150	0^	0^
Adjusted Baseline Gross Plunger Stroke (in)	N/A	N/A	47	46	42	48	43

* Program Output Value
^ Value Forced by Program Boundary Conditions

Table 4
Program Output Comparisons
Case 3

Item	DHLC	A	B	C	D	E	F	G
			MODELS					
Gearbox %	-	N/A	98	93	95	97	101	77
Unit %	-	78	78	81	79	79	81	74
PRHP (hp)	-	N/A	10.0	10.3	10.9	11.7	10.3	11.5
PPRL (lbs)	19587	19587	19587	19884	19731	19646	19954	18401
MPRL (lbs)	7738	7738	7738	7942	6941	7077	6713	8351
SPM	11.0	11.0	11.0	10.6	11.2	11.2	10.6	11.0
1" SR %	-	72	71	73	76	74	77	62
7/8" SR %	-	78	75	80	85	76	80	62
3/4" SR %	88	85	81	83	88	78	83	62
Pump Stroke								
Gross (in)	-	71	69	74	74	79	79	75
Net (in)	-	N/A	66	72	N/A	N/A	76	N/A
PPIP (psi)	385	1290*	100	178*	408	408	178	408

* Calculated by Program

Item	DHLC	A	B	C	D	E	F
Bottom Min Stress (psi)	-3200	-7175*	-4004*	-3773	-3528	-3098*	-3757
Dynamic Min Stress (psi)	-339	-4315	-1144	-913	-668*	-238	-897
Bottom Min Force (lbs)	-1414	-3170	-1769	-1667*	-1559	-1369	-1660*
Dynamic Force (lbs)	-150*	-1906	-505	-403	-295	-105	-396
Dynamic Force (lbs)	-150	-250	-150	-220	-100	0^	0^
Adjusted Baseline Gross Plunger Stroke (in)	N/A	76	73	78	74	79	70

* Program Output Value
^ Value Forced by Program Boundary Conditions

Table 5
Program Output Comparisons
Case 4

Item	DHLC	A	B	C	D	E	F	G
			MODELS					
Gearbox %	-	-	103	107	101	-	103	94
Unit %	-	-	70	67	67	-	65	67
PRHP (hp)	-	-	34.3	33.9	35.0	-	N/A	32.3
PPRL (lbs)	25645	-	25645	24314	24592	-	23902	24284
MPRL (lbs)	6218	-	6218	4768	4249	-	3703	6180
SPM	9.0	-	9.0	8.9	9.0	-	8.9	8.9
1" HS %	-	-	62	68	63	-	69	63
7/8" HS %	-	-	67	70	66	-	70	63
3/4" HS %	64	-	76	77	67	-	68	63
Pump Stroke								
Gross (in)	-	-	156	156	149	-	151	149
Net (in)	-	-	N/A	150	N/A	-	151	N/A
PPIP (psi)	109	-	84	195*	109	-	195	109

* Calculated by Program

Item	DHLC	A	B	C	D	E	F
Bottom Min Stress (psi)	-3090	N/A	-1837*	-1864	-3444	-2806*	-3672
Dynamic Min Stress (psi)	-566	N/A	687	660	-920*	-282	-1148
Bottom Min Force (lbs)	-1365	N/A	-812	-824*	-1522	-1240	-1623*
Dynamic Force (lbs)	-300*	N/A	304	292	-406	-125	-507
Dynamic Force (lbs)	-300	N/A	-450	-540	-200	0^	0^
Adjusted Baseline Gross Plunger Stroke (in)	N/A	N/A	156	156	149	N/A	151

* Program Output Value
^ Value Forced by Program Boundary Conditions

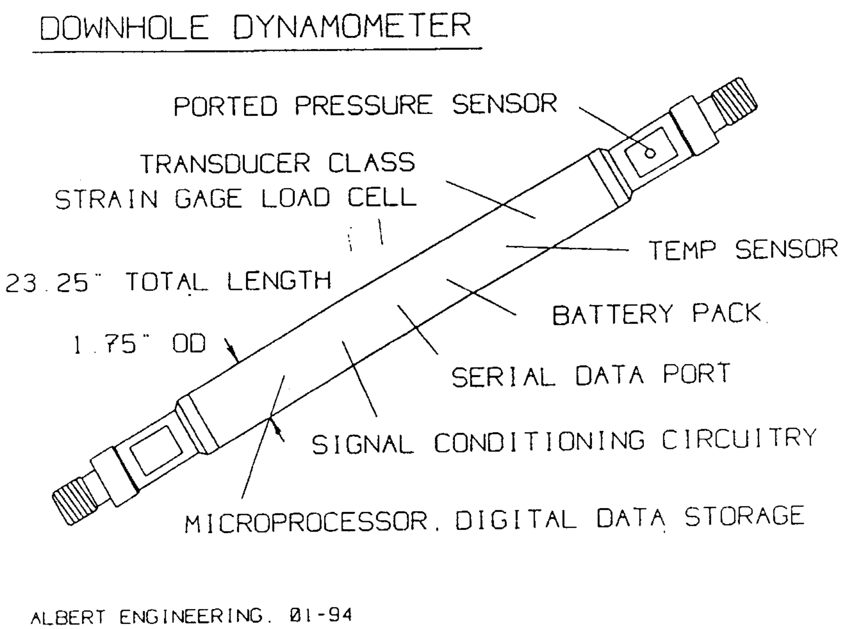

Figure 1 - Downhole dynamometer

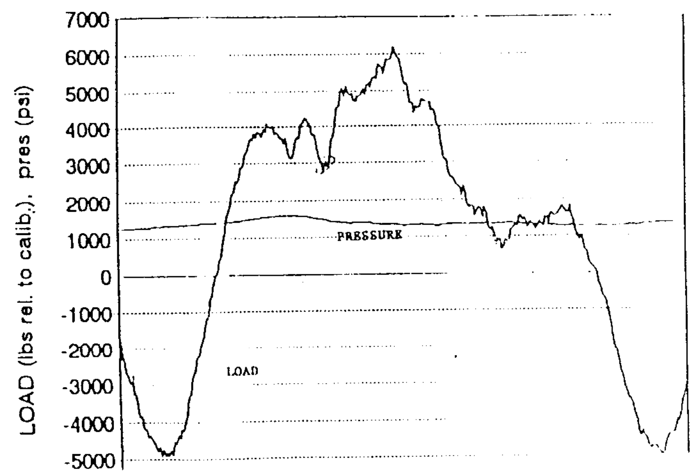

Figure 3 - Case #1 - Mid-string

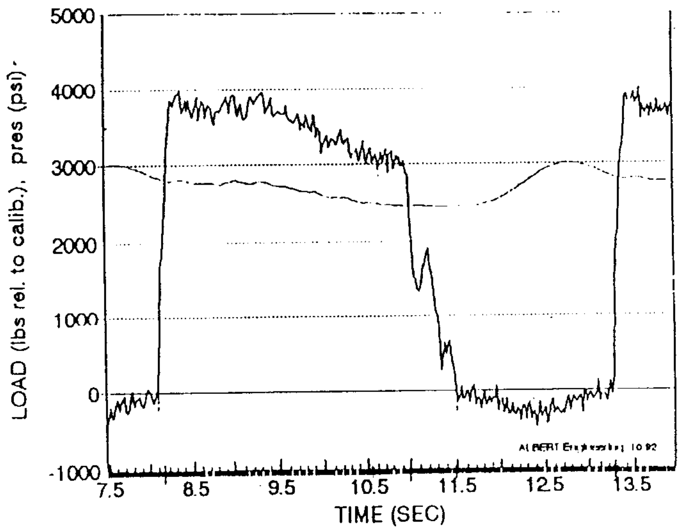

Figure 2 - Case #1 - Downhole

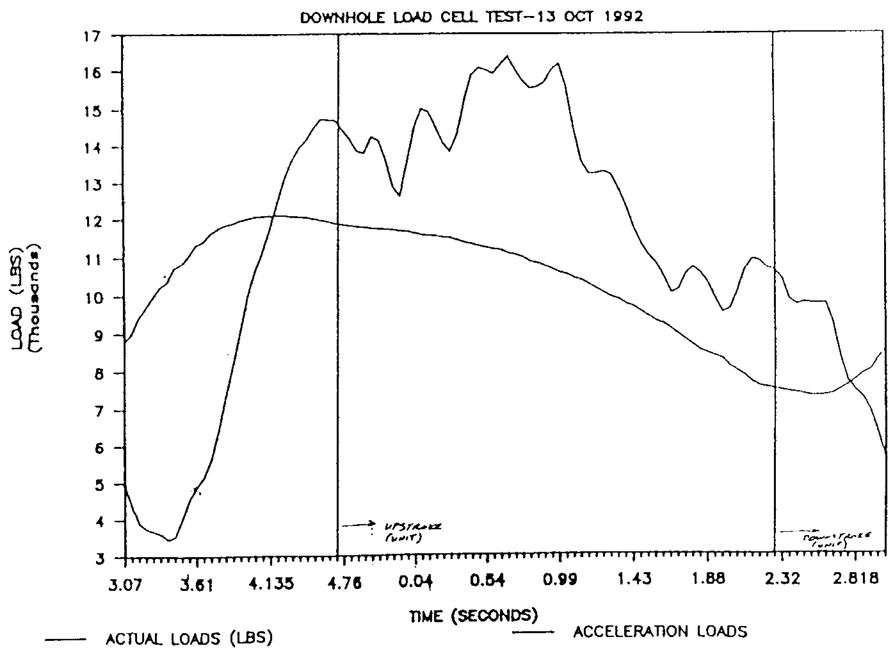

Figure 4 - Case #1 - Surface

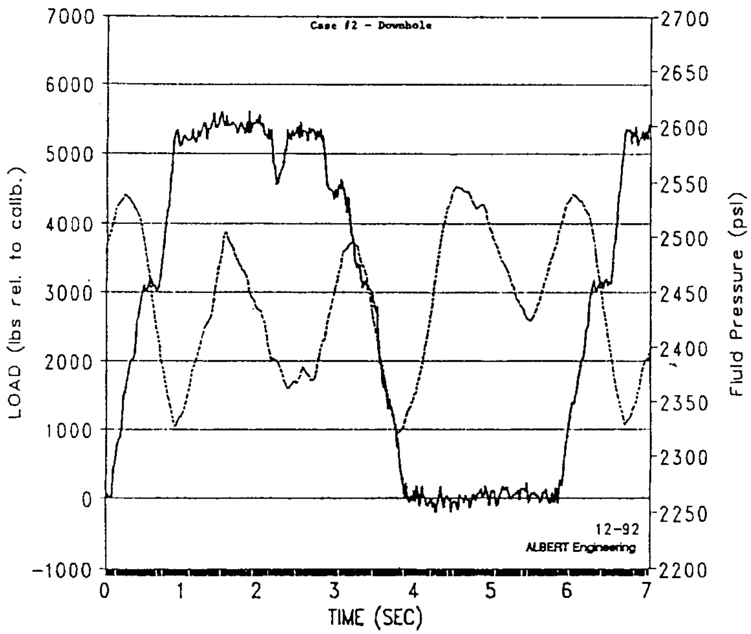

Figure 5 - Case #2 - Downhole

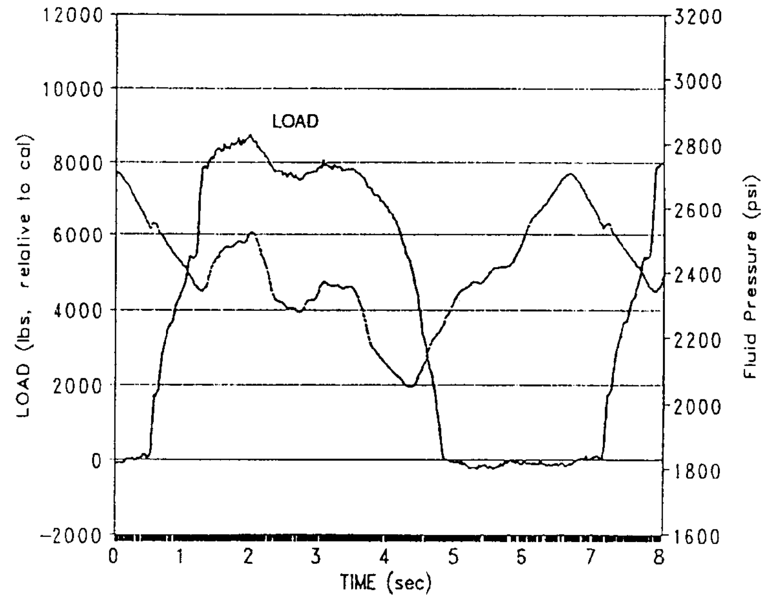

Figure 7 - Case #4 - Downhole

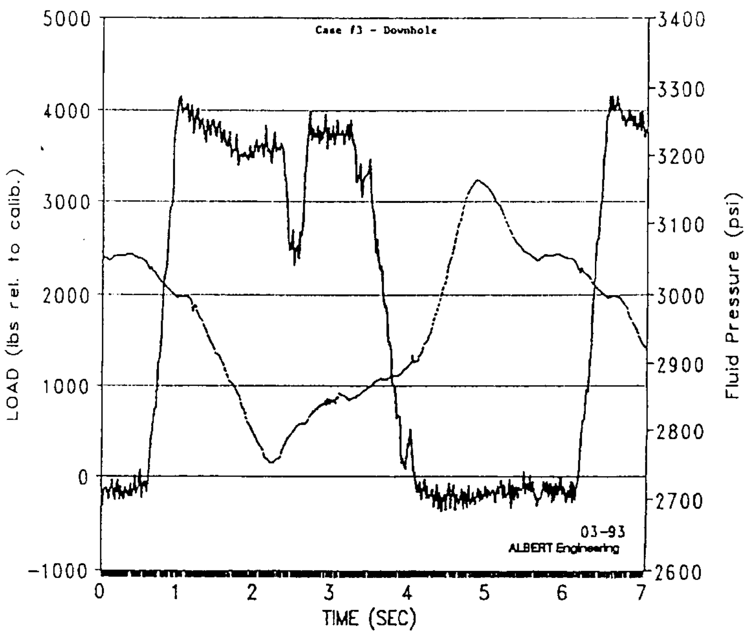

Figure 6 - Case #3 - Downhole

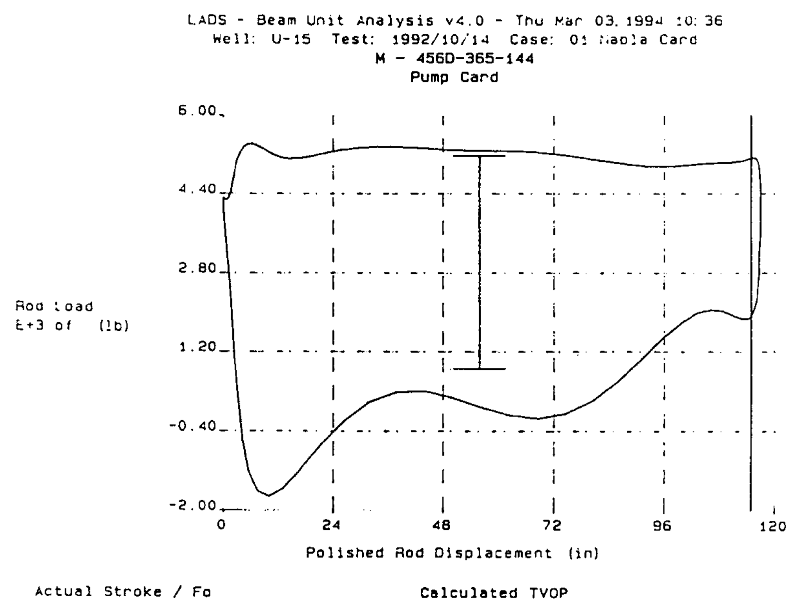

Figure 8